GA–A27437

SCALING OF THE DIVERTOR HEAT FLUX WIDTH IN THE DIII-D TOKAMAK

by
M.A. MAKOWSKI, A.W. LEONARD, J.D. ELDER,
C.J. LASNIER, J. NICHOLS, T.H. OSBORNE,
P.C. STANGEBY and J.G. WATKINS

OCTOBER 2012

GENERAL ATOMICS

DISCLAIMER

GA–A27437

SCALING OF THE DIVERTOR HEAT FLUX WIDTH IN THE DIII-D TOKAMAK

by
M.A. MAKOWSKI,[1] A.W. LEONARD, J.D. ELDER,[2]
C.J. LASNIER,[1] J. NICHOLS,[3] T.H. OSBORNE,
P.C. STANGEBY[2] and J.G. WATKINS[4]

This is a preprint of a paper to be presented at the 24th IAEA Fusion Energy Conference, October 8–13, 2012 in San Diego, California and to be published in the Proceedings.

[1]Lawrence Livermore National Laboratory, Livermore, California USA
[2]University of Toronto Institute for Aerospace Studies, Toronto, Canada
[3]Princeton Plasma Physics Laboratory, Princeton, New Jersey USA
[4]Sandia National Laboratories, Albuquerque, New Mexico USA

Work supported by the
U.S. Department of Energy under
DE-AC52-07NA27344, DE-FC02-04ER54698,
DE-AC02-09CH11466 and DE-AC04-94AL85000

GENERAL ATOMICS PROJECT 30200
OCTOBER 2012

ABSTRACT

Significant progress has been made in the study of the divertor heat flux width and how it relates to upstream scrape-off-layer (SOL) profiles, as well as how these profiles relate to stability properties at or near the separatrix. On DIII-D this has been made possible by an upgrade to the Thomson scattering system that provides highly resolved profiles in both space and time. The upstream separatrix pressure is found to scale with the pressure at the divertor target plate as measured by the Langmuir probe array. This provides confirmation that pressure is conserved along a field line. Recent multi-machine studies have found that the heat flux width scales as I_p^{-1} where I_p is the plasma current (or equivalently with B_p^{-1} where B_p is the poloidal magnetic field at the outer midplane), with minor dependences on other parameters, and significantly, independent of machine size. This simple result greatly reduces the number of viable theoretical models of the heat flux width. Critical pressure gradient models form one such class in which the gradient scale length is set by edge turbulence induced by MHD instabilities in analogy with the kinetic ballooning mode (KBM) paradigm for the pedestal gradient. Here the critical gradient is posited to extend all the way to the separatrix and possibly into the SOL. We find strong support for this type of model in that, for several parametric scans, the measured separatrix pressure gradient scales in concert with the infinite-*n* critical pressure gradient from the BALOO code, which serves as a proxy for the stability of the KBM (or possibly the resistive ballooning mode). In addition, Langmuir probe data also yields a measurement of the peak heat flux that reproduces the trends observed with the IRTV diagnostic.

1. INTRODUCTION

The heat flux width is a critical design parameter for the divertor in ITER and other next generation devices, as it determines the peak thermal loading to the divertor target plate. ITER requires that the divertor be operated in a partially detached regime in order to maintain the heat flux below the maximum steady-state heat load of 10 MW/m^2 [1] set by material limits. Understanding how the heat flux width scales with plasma and engineering parameters is thus essential for the successful operation of the ITER divertor. Much progress has recently been made on this topic [2–4] with the result that the heat flux width is found to be strongly dependent on the inverse of the poloidal magnetic field at the outer midplane separatrix, essentially independent of machine size, and weakly dependent on injected power. This leads to projections of the heat flux width for ITER of ~1 mm, which is approximately five times smaller than the current ITER design value.

Even though the scaling of the heat flux width now appears to be established, the physics behind it is still not well understood. To increase the confidence of extrapolation, a physical model describing this scaling is needed. In order to make the connection between the two a knowledge of the edge parameters, both in the pedestal and scrape-off-layer (SOL), is needed. High resolution profile measurements of the electron temperature and density are now routine on DIII-D with the advent of an upgraded Thomson scattering system featuring both improved spatial resolution, provided by additional edge channels, and improved temporal resolution, provided by additional lasers. The spatial resolution has been increased further by modulating the location of the separatrix where it intersects the Thomson chord. We have obtained high-resolution Thomson profiles as a function of plasma current, density, injected power, and upper triangularity.

With the insight provided by a well-established empirical scaling law combined with the detailed profile measurements, we are in a position to make detailed comparisons to physics based theoretical models for the heat flux width. In Section 2, results of heat flux scaling studies in DIII-D are reported in on with the result that the heat flux width is dependent solely on the inverse of the midplane poloidal field. Upstream profiles are discussed in Section 3 where it is found that the gradient scale length is primarily dependent on the density scale length. Section 4 examines the evidence in support of critical gradient models setting the heat flux width. The critical gradient found from the BALOO code scales with separatrix pressure gradient, supporting this model. Finally, Section 5 concludes with a summary of the results of this work.

2. SCALING OF THE HEAT FLUX WIDTH ON DIII-D

The heat flux profile is measured with infrared thermography [5] and mapped to the outer midplane. Mapping to a standardized location facilitates inter-machine comparison of devices with different divertor geometries as well as comparison of profiles obtained on the same machine when the magnetic configuration is varied. The heat flux profile is generally characterized by a single scalar value, the heat flux width. Traditionally, the integral width (integral of the profile divided by the peak value) is used for this characterization [6]. However, Eich [4] has developed a two-parameter semi-empirical fitting function that very accurately describes the full profile. One parameter governs the profile in the private flux region and corresponds to a Gaussian width, w_{pvt}, while the other governs the profile in the SOL and corresponds to an exponential decay length, λ_{sol}. The integral width for this functional form is found to be a linear combination of the private flux and SOL widths [3] with $\lambda_{\text{int}} \cong \lambda_{sol} + 1.64 w_{pvt}$. However, by independently regressing the two parameters, w_{pvt} and λ_{sol}, it is possible to determine how each of them varies since the physics in the two regions is likely to differ [3].

Heat flux width measurements have been obtained as a function of plasma current (I_p) and toroidal field (B_t) [7], normalized density (Greenwald fraction, f_G), injected power (P_{inj}), and upper triangularity (δ_u). All data was acquired in ELMy H-mode with an attached divertor. Regression analysis against an assumed power law scaling of the form

$$\lambda = C \cdot I_p^{e_I} B_t^{e_B} f_G^{e_f} P_{inj}^{e_P} \delta_u^{e_\delta} L_{conn}^{e_L} \tag{1}$$

where L_{conn} is the connection length, has been made and results in a strong inverse dependence on I_p and weak dependencies on the other parameters. It is found that the correlation is improved by replacing I_p with $B_{p,mp}$, the poloidal field at the outer midplane. The result for the SOL decay length is a scaling strongly dependent on $B_{p,mp}$, weakly dependent on δ_u, and independent of all other parameters. The I_p dependence for DIII-D was first reported on in [8]. Results of the regression analysis are shown in Fig. 1 and are consistent with the available multi-machine databases on heat flux width [2,3]. For comparison, the regression results for a scaling with all parameters included are listed in Table I together with the corresponding F-statistic. For the results to be statistically significant, the F-statistic should be well above 3.

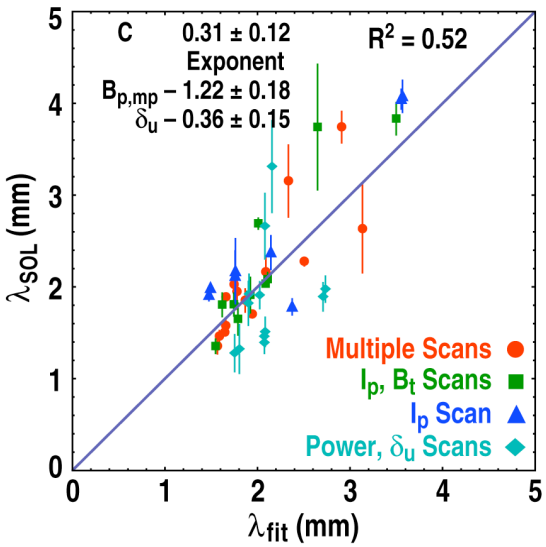

FIG. 1. Regression analysis for the SOL decay length parameter, λ_{sol}. The only significant scaling parameters are $B_{p,mp}$ and δ_u.

Table I
Regression results for power law scaling with all parameters included together with their corresponding *F*-statistic

Parameter	Range	*F*-statistic
C	0.50 ± 0.34	—
$B_{p,mp}$	-1.11 ± 0.71	39.5
B_t	-0.25 ± 0.63	0.17
f_G	-0.21 ± 0.31	1.76
P_{inj}	-0.05 ± 0.09	1.04
δ_u	-0.30 ± 0.17	3.30
L_{conn}	0.03 ± 0.58	1.89×10^{-3}

A similar analysis for the private flux Gaussian width, w_{pvt}, yields the result $w_{pvt} = 0.31 B_{p,mp}^{-1.19 \pm 0.21}$ with a correlation coefficient of 0.42. There is again a robust inverse dependence on $B_{p,mp}$. However, the dependence on other parameter is rather weaker and the exponents fluctuate with the choice of secondary parameters, although the signs of the exponents do not do so. Intuitively, one would expect that the private flux width should increase with increasing diffusion time, which in turn should increase with increasing connection length, L_{conn}. However, no such dependence is found in this data set ($e_L \sim 0$).

Figure 2 plots a variety of parameters versus two of the scan parameters δ_u [Fig. 2(a,c,e), left column] and P_{inj} [Fig. 2(b,d,e), right column] with all other parameters fixed. Figure 2(a,b) plots the peak parallel heat flux as measured by the IRTV and Langmuir probe array (LPA). The two measurements are in agreement in both trend and magnitude, although the LPA is about 1.5–2 times larger than the IRTV value. This is well within the experimental measurement error. Pedestal $\beta_{e,pol}$ and the electron pressure at the separatrix as measured by Thomson scattering and the LPA are plotted in Fig. 2(c,d). Here, $\beta_{e,pol}$ increases with δ_u, as expected, while the Thompson and LPA separatrix pressure are independent of δ_u. In contrast, $\beta_{e,pol}$ is nearly independent of P_{inj} while the Thomson and LPA separatrix pressure both increase with increasing P_{inj}. The upstream Thomson separatrix pressure is nearly equal to twice the LPA separatrix pressure, consistent with sonic flow at the target, and the two trend proportionately to one another in both scans. Assuming, the $T_i = T_e$, the excellent agreement between upstream and target separatrix pressures implies that the separatrix location is correctly chosen. Figure 2(e,f) plots the heat flux widths (λ_{sol}, w_{pvt}, and λ_{int}) versus δ_u. The decrease in λ_{sol} and λ_{int} with increasing δ_u is quite evident while w_{pvt} is essentially independent of δ_u. All widths increase with increasing P_{inj}, although w_{pvt} displays the weakest dependence.

These trends can also be seen in Fig. 2(g,h). Here, the heat flux profiles for the extreme values (low: solid red line; high: dashed green line) of the δ_u and P_{inj} scans are plotted versus relative midplane major radius. For the δ_u scan, the profile narrows slightly and remains nearly constant in amplitude as δ_u is increased. The areas are nearly equal indicating that the total power $= 2\pi R q_0 \lambda_{\text{int}}$ is also approximately constant, consistent with the trends of q_0 [Fig. 2(a);

increasing] and λ_{int} [Fig. 2(e); decreasing]. For the P_{inj} scan, the trends in heat flux width and peak heat flux are again expressed in the raw profiles (note the scale difference between the two curves). As P_{inj} increases, both the width and amplitude of the profile increase, consistent with the q_0 and λ_{int} trends with P_{inj} (both increasing with increasing P_{inj}).

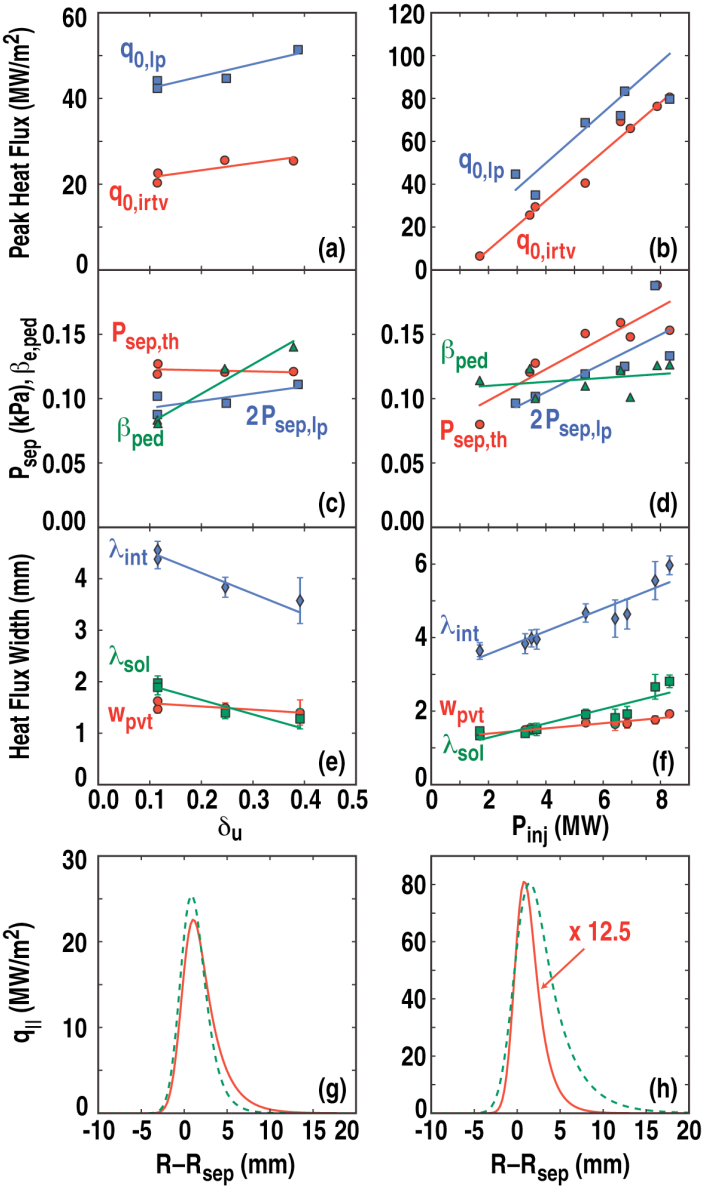

FIG. 2. (a,b) Plots of peak heat flux as measured by IRTV (red circles) and Langmuir probes (blue squares) versus δ_u (left) and P_{inj} (right). (c,d) pedestal poloidal electron beta (green triangles) and separatrix electron pressure as measured by IRTV (red circles) and Langmuir probes (blue squares). (e,f) heat flux widths [λ_{sol} (green squares), w_{pvt} (red circles), and λ_{int} (blue diamonds)]. (g,h) Plots of fits to the heat flux profiles at the extreme values of the δ_u scan [left column] and P_{inj} scan [right column] versus the relative mid-plane major radius.

The dependence of λ_{sol} on δ_u in the scaling law of Section 2 is reflected in the raw data Fig. 2(e) (green squares), i.e. decreasing with increasing δ_u. However, the increase in the heat flux width with increasing P_{inj} is not echoed in the scaling relation for the full data set. The reason for this is not clear, but seems to result from the scatter at low power where a majority of the data was acquired. Regression of the P_{inj} scan data alone yields $w_{pvt} \sim P_{inj}^{0.24}$, $\lambda_{sol} \sim P_{inj}^{0.46}$, and $\lambda_{int} \sim P_{inj}^{0.32}$. Also, imposing a P_{inj} dependence on the data by regressing against $\lambda_{sol} / P_{inj}^{0.46}$ results

in the scaling $\sim B_{p,mp}^{-1.39}\delta_u^{-0.43}$ with $R^2 = 0.477$, which is similar to the scaling of Fig. 1 but with a somewhat lower correlation coefficient. Thus a P_{inj} dependence is not completely ruled out. That the heat flux width is nearly independent of P_{inj}, is consistent with other multi-machine studies [2]. We also note that the decrease in heat flux width with δ_u is anti-correlated with the pedestal electron poloidal beta, $\beta_{e,ped,pol}$, which increases almost a factor of 2 (due almost entirely to an increase in the pedestal density as show below in Fig. 3) as δ_u increases from 0.1 to 0.4. This is not in conflict with the P_{sep} scaling results as $\beta_{e,ped,pol}$ depends on the global poloidal stability, while P_{sep} results from a highly localized measurement. For the P_{inj} scan, $\beta_{e,ped,pol}$ is nearly constant while P_{sep} increases in concert with the peak heat flux. This suggests that the pedestal pressure (or equivalently β_{ped}) is not simply related to that in the separatrix/SOL region. However, it does appear that P_{sep} is highly correlated with the peak heat flux. Note that the P_{sep} results are dependent on the exact location of the separatrix, which is subject to some uncertainty as described in Section 4.

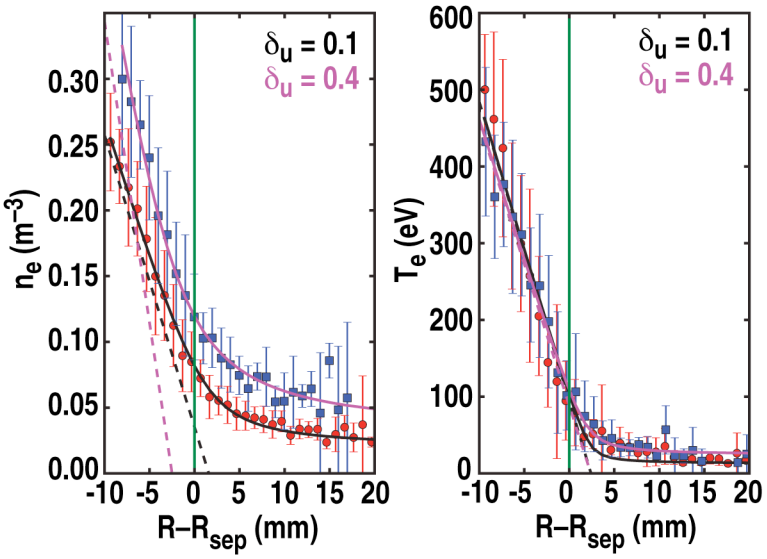

FIG. 3. Plot of electron density and temperature profiles for the extreme values of the δ_u scan of Fig. 2. The change in the pressure gradient scale length is due entirely to the change in the density gradient scale length.

3. EDGE PROFILES

In order to make a connection between the heat flux width and models of parallel transport in the SOL considered below, detailed measurements of the edge profiles are needed. These are provided by an upgraded Thomson scattering system that features improved spatial resolution through an increased number of channels in the vicinity of the separatrix as well as improved time resolution provided by additional lasers. The spatial resolution is further increased by modulating the position of the separatrix, where it intersects the vertical Thomson chord. When mapped to the outer midplane, this yields millimeter-scale resolution of the electron profiles.

We have obtained detailed edge profiles of electron temperature and density for all of the heat flux parameter scans. An example is shown in Fig. 3, which plots the electron density and temperature profiles for the extreme values of the δ_u scan of Fig. 2. Since

$$\frac{1}{L_{P_e}} = \frac{1}{L_{n_e}} + \frac{1}{L_{T_e}} \tag{2}$$

where

$$L_u = \left(\frac{1}{u} \frac{du}{dR} \right)^{-1} \tag{3}$$

it is clear from Fig. 3 that the change in the pressure gradient scale length is due entirely to the change in the density gradient scale length and is attributable to an increase in density rather than a decrease in the density gradient. This is generally the case: the change in the density scale length dominates the change in the pressure scale length as a function of I_p, δ_u, and n_e. The P_{inj} scan is exceptional in this regard in that changes in the both density and temperature profiles contribute to changes in the pressure scale length.

4. CRITICAL GRADIENT MODELS FOR THE HEAT FLUX WIDTH

Above we have found that the primary dependence of the heat flux width is on $B_{p,mp}$. This fact greatly restricts the number of viable theoretical models of the physics setting the heat flux width. Good candidates are critical pressure gradient models in which the gradient scale length is set by edge turbulence induced by MHD instabilities in analogy with the kinetic ballooning mode (KBM) paradigm for the pedestal gradient [9]. In particular it is posited that the critical gradient extends all the way to the separatrix and possibly into the SOL [10,11]. Contact with the experimentally observed $B_{p,mp}$ dependence is made through the α-parameter that arises in the theory, where $\alpha = RP'q^2 / B_t^2 \sim P' / I_p^2 \sim P' / B_p^2$, R is major radius, P' is the pressure gradient, and q is the safety factor. In the case of the heat flux width, the pressure gradient at the separatrix is of particular interest.

The question of the exact location of the separatrix is a thorny one in its own right. For the data presented in this paper, we define the separatrix as the location of the symmetry point of a tanh-function fit to the electron temperature profile plus one-half of the SOL temperature decay length [12] and estimate the error in the separatrix location as ±2 mm. However, even this small variation in location leads to large variations in the separatrix pressure gradient as the location falls in the steep gradient region of the profiles (see Fig. 3). In order to circumvent this issue, we also evaluate the gradients at $\psi = 1 \pm 0.001$, where ψ is the normalized flux, to estimate the error, and find that the trends are generally independent of the ψ-value chosen. However, different definitions of the separatrix location can lead to differing dependencies as discussed next.

Figure 4(a,b) plots the total pressure gradient (assuming $P_e = P_i$) evaluated at the separatrix (defined as the foot of the electron temperature profile) versus δ_u [Fig. 4(a,c)] and P_{inj} [Fig. 4(b,d)] together with the critical pressure gradient for the infinite-n ideal ballooning limit obtained from the BALOO code [13]. Here, the infinite-n critical gradient is used as a proxy for the stability of the kinetic ballooning mode. Two regions of instability are generally found that are separated by a second stable region roughly corresponding to the location of the pedestal.

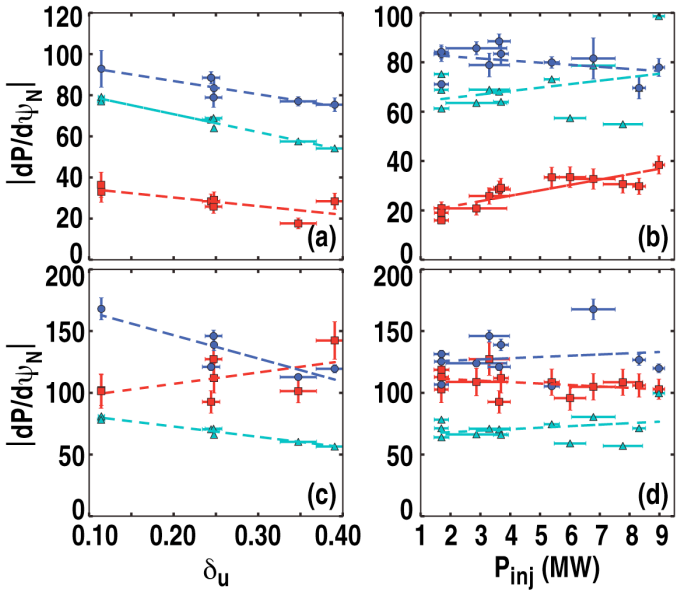

FIG. 4. (a,b) P'_{meas} (red squares), $P'_{crit,core}$ (cyan triangles), $P'_{crit,edge}$ (blue circles) versus δ_u (a,c) and P_{inj} (b,d). Separatrix defined as the foot of the electron temperature profile [12]. (c,d) Same as (a,b), but separatrix defined as the foot of the electron pressure profile.

For each value in the scan, two BALOO points are obtained by extrapolating the first stability boundary of each of these regions to the separatrix: the core region (cyan triangles) and the extreme edge region (blue circles). The core extrapolated stability limit trends with the measured pressure gradient for both scans. The trend from the edge extrapolated stability limit is in agreement with the δ_u scan data, but weakly counter to the P_{inj} scan data. Also, the measured pressure gradient falls well below the infinite-n limit. This is not unexpected as resistive corrections at the separatrix will reduce P'_{crit}. Figure 4(c,d) plots are the same as (a,b) but with the separatrix location corresponding to the foot of the electron *pressure* profile. The pressure foot lies at smaller major radius and thus at larger values of density and temperature and in a region of steeper gradients (see Fig. 3). This modifies the trends for the δ_u scan. Here the measured separatrix pressure gradient increases with increasing δ_u, but the extrapolated pressure limits still decrease. The trends for the P_{inj} scan are somewhat weaker, but essentially the same. However, both the measured pressure gradient and extrapolated stability limits increase relative to those of the upper traces [Fig. 4(a,b)], with the measured pressure gradient about equal to the calculated stability limit. The pressure foot separatrix location is likely at too small a major radius to be physical. However, this demonstrates the importance of accurately determining the separatrix location.

In [3] the core extrapolated BALOO critical pressure gradient also trended proportionately with the measures separatrix pressure for an I_p-scan. When combined with the scans in Fig. 4, these results strongly support the critical gradient model for the heat flux width. However, it is unclear whether the KBM or another mode is responsible for inducing transport that establishes the heat flux width.

5. RESULTS AND CONCLUSIONS

Scaling studies reveal that the heat flux depends essentially only on I_p (or equivalently on $B_{p,mp}$). Secondary dependencies are observed but invariably are much weaker. Remarkably, the multi-machine scaling results display little dependence on size, either major and minor radius. A modest dependence of the heat flux width on δ_u is obtained for the DIII-D data set consistent with a scan with all other parameters held constant. A similar scan versus P_{inj} also shows a trend when all other parameters are held fixed. However, the trend does not persist in the full data set.

The edge diagnostic set is providing a compelling picture of the physics at the separatrix and in the SOL. Detailed measurements of the upstream profiles with the upgraded Thomson scattering system have provided high quality measurement of electron temperature, density, and pressure, making comparison with theoretical models possible. Good correlations in both trend and magnitude (within a factor of 2) are observed between the upstream separatrix pressure and that measured at the divertor target with the LPA, indicating that pressure conservation is obtained along a field line in agreement with edge modeling results and theoretical considerations. Good agreement in both trend and relative magnitude (within a factor of 2) between the LPA and IRTV measurements of the peak heat flux is also obtained.

Significant progress on the physics setting the heat flux width has also been made. The most significant result is that the infinite-*n* ballooning mode critical pressure gradient scales with the measured separatrix pressure gradient, where the separatrix is defined as in [12]. This is a robust result as agreement has now been obtained for three independent parameter scans and strongly suggests that some form of critical gradient physics is implicated in setting the heat flux width.

REFERENCES

[1] LINKE, J., Trans. Fusion Sci. Technol. **49** (2006) 455.

[2] EICH, T., *et al.*, "Scaling of the tokamak near scrape-off layer H-mode power width and implications for ITER", this conference, paper ITR/1-1.

[3] MAKOWSKI, M.A., *et al.*, Phys. Plasmas **19** (2012) 056122.

[4] EICH, T., *et al.*, Phys. Rev. Lett. **107** (2011) 215001.

[5] HILL, D.N., *et al.*, Rev. Sci. Instrum. **59** (1988) 1878.

[6] LOARTE, A., *et al.*, Nucl. Fusion **47** (2007) S203-S263.

[7] MAKOWSKI, M.A., J. Nucl. Mater. **415** (2011) S357-S359.

[8] LASNIER, C.J *et al.*, Nucl. Fusion **38** (1998) 1225.

[9] SNYDER, P.B., *et al.*, Nucl. Fusion **51** (2011) 103016.

[10] LaBOMBARD, B., *et al.*, Phys. Plasmas **15** (2008) 056106.

[11] LaBOMBARD, B., *et al.*, Phys. Plasmas **18** (2011) 056104.

[12] PORTER, G.D. *et al.*, Phys. Plasmas **5** (1998) 1410.

[13] HONG, B.G., *et al.*, Phys. Fluids B **1** (1989) 1589.

ACKNOWLEDGMENT

This work was supported in part by the U.S. Department of Energy under DE-AC52-07NA27344, DE-FC02-04ER54698, DE-AC02-09CH11466 and DE-AC04-94AL85000.